

A Heat-Activated Drug-Delivery Platform Based on Phosphatidyl-(oligo)-glycerol Nanocarrier for Effective Cancer Treatment

Martin Hossann, Johannes Hirschberger, Rebecca Schmidt, Christine Baumgartner, Katja Zimmermann, Silke Baer, Christina Ratzlaff, Michael Peller, Karin Troedson, Simone Limmer, Andreas Brühshwein, Rene Dörfelt, Nina Kreuzmann, Gerhard Wess, Thomas Knösel, Olaf Schagon, Johannes Fischer, Holger Grill, Linus Willerding, Michael Schmidt, Andrea Meyer-Lindenberg, Rolf D. Issels, Markus Schwaiger, Alexander M. Eggermont, Timo L. ten Hagen, and Lars H. Lindner*


The potential of cancer drugs is not fully exploited due to low tumor uptake and occurrence of systemic side effects, limiting maximum tolerated dose. Actively targeted nanocarriers improve efficacy while minimizing off-target toxicity. Herein, it is the first time a drug-delivery platform for heat-triggered intravascular drug release is described, based on synthetic phosphatidyl-(oligo)-glycerols from organic synthesis to preclinical investigation in feline patients. For the nanocarrier formulated doxorubicin (DOX), superior tumor drug delivery and anti-tumor activity compared with free DOX, conventional liposomal DOX (Caelyx), and temperature-sensitive lysolipid-containing DOX-liposomes in rat sarcoma are demonstrated. In a comparative oncological study with neoadjuvant treatment of feline sarcoma, a metabolic response determined with ^{18}F -FDG-positron emission tomography/magnetic resonance imaging (PET/MRI) and histopathological response after tumor resection are significantly better compared with free DOX, potentially by overcoming drug resistance based on improved intratumoral drug distribution. This novel drug-delivery platform has great potential for the treatment of locally advanced tumors in humans.

1. Introduction

Soft tissue sarcoma (STS) accounts for less than 1% of all malignancies with about 13 000 new cases per year in the United States, and more than 5300 people die of these tumors annually. Most STS grow asymptotically, either at the extremities or as abdominal/retroperitoneal tumors and are diagnosed at advanced stages. Surgery with the goal of clear margins, and the addition of radiotherapy for extremity STS, represent the mainstay of local therapy. For extremity STS, where blood vessels and nerves are involved, this is frequently accomplished with relevant functional deficits. For retroperitoneal STS, compartmental resections with the removal of adjacent organs are required. Despite extended surgery, the local recurrence rate remains high with up to 50% recurrence in 5 years.^[1]

Dr. M. Hossann, Dr. R. Schmidt, Dr. S. Limmer, Dr. L. Willerding,
Prof. R. D. Issels, Prof. L. H. Lindner
Department of Medicine III & Sarcoma Center (SarkUM)
University Hospital
LMU Munich
Marchioninistraße 15, 81377 Munich, Germany
E-mail: lars.lindner@med.uni-muenchen.de

Dr. M. Hossann
Thermosome GmbH
82152 Planegg/Martinsried, Germany

 The ORCID identification number(s) for the author(s) of this article can be found under <https://doi.org/10.1002/anbr.202000089>.

© 2021 The Authors. Advanced NanoBiomed Research published by Wiley-VCH GmbH. This is an open access article under the terms of the Creative Commons Attribution License, which permits use, distribution and reproduction in any medium, provided the original work is properly cited.

DOI: 10.1002/anbr.202000089

Prof. J. Hirschberger, Dr. K. Zimmermann, S. Baer, C. Ratzlaff,
Dr. K. Troedson, Dr. R. Dörfelt, Dr. N. Kreuzmann, Prof. G. Wess
Clinic of Small Animal Medicine
LMU Munich
Veterinärstr. 13, 80539 Munich, Germany

Dr. C. Baumgartner, Dr. J. Fischer, Prof. M. Schwaiger
Department of Nuclear Medicine
Klinikum Rechts der Isar
Ismaninger Straße 22, 81675 Munich, Germany

Dr. M. Peller
Department of Radiology
University Hospital
LMU Munich
Marchioninstr. 15, 81377 Munich, Germany

Dr. A. Brühshwein, Prof. A. Meyer-Lindenberg
Clinic of Small Animal Surgery and Reproduction
LMU Munich
Veterinärstr. 13, 80539 Munich, Germany

Since their discovery in the seventies, anthracyclines (ATC), such as doxorubicin (DOX) and epirubicin, remain the most active chemotherapeutic drugs for the treatment of STS. Moreover, neoadjuvant ATC-based combination chemotherapy for locally advanced high-risk STS has recently been shown to improve overall survival when compared with various other chemotherapeutic drugs.^[2] The main objective for neoadjuvant chemotherapy is downsizing the tumor to facilitate surgical resection. However, current response rates are less than 30%,^[2,3] and almost 10% of patients progress under neoadjuvant treatment.

Response to ATC-based combination chemotherapy is improved by adding regional hyperthermia (RHT) to the treatment scheme, where the tumor and the surrounding tissue are simultaneously heated to 40–43 °C for 60 min with the use of a radiofrequency applicator. Hyperthermia has been shown to act synergistically with a multifactorial mode of action, among others, by increasing tissue perfusion, drug extravasation, and uptake.^[4] Within a randomized phase III trial, response and subsequent survival of patients treated with neoadjuvant chemotherapy plus RHT were significantly improved compared with patients treated with chemotherapy alone.^[3,5]

The effectiveness of anticancer drugs in treating a solid tumor is generally dependent on delivery of the drug to virtually all cancer cells in the tumor. However, intravenously applied DOX is especially incapable of penetrating cells beyond the vicinity of the vasculature.^[6] Higher dosing, to overcome this limitation, is prevented by systemic side effects and therefore the clinical recommended dose is not reflective of the most effective dose regarding antitumor efficacy. Response rates for conventional DOX as monotherapy are remarkably low with 10–20%, and 20–30% of patients progress under therapy.^[7–9]

Nanocarriers such as liposomes have been extensively explored for improved drug delivery.^[10] Especially PEGylated and thus long-circulating liposomes should prevent the intravenously administered drug from a rapid systemic distribution, but primarily transport the drug into the tumor by passive accumulation due to the increased permeability and retention effect (EPR). However, clinical studies demonstrated that liposomal encapsulation of DOX contributed primarily to a decreased toxicity profile^[11] rather than improved efficacy.^[12,13] Reasons for the latter are manifold. The extravasation of the liposomal nanocarrier from leaky tumor vasculature is a heterogeneous and variable process among different tumor types,^[14,15] and recent studies indicate that the EPR effect for nanoparticle

delivery has been overestimated^[14] or might not even be the root cause.^[16] Importantly, the encapsulated drug doesn't become fully bioavailable even if the liposome reaches the tumor.^[17]

Liposomes, which instantly release their payload through a specific trigger, can circumvent the problem of reduced bioavailability, with thermosensitive liposomes (TSL) being the most promising technology.^[10] While being first described by Yatvin et al.,^[18] multiple TSL formulations have been developed in the recent decades to improve, e.g., bioavailability and stability.^[19] TSL composed of 1,2-dipalmitoyl-*sn*-glycero-3-phosphocholine (DPPC), 1-stearoyl-*sn*-glycero-3-phosphocholine (S-Lyso-PC), and 1,2-distearoyl-*sn*-glycero-3-phosphoethanolamine-N-methoxy(PEG)-2000 (DSPE-PEG2000, **Figure 1A**) is the most advanced formulation (LTSL) and currently in clinical testing.^[20] The formulation failed to reach its primary endpoint in a phase III clinical trial for the treatment of liver cancer in combination with radiofrequency ablation (HEAT, NCT00617981), whereas a subgroup analysis of patients with prolonged heating time showed superiority. However, the OPTIMA study (NCT02112656) conducted as a result was also stopped for futility. The possible reasons for failure include both formulation aspects and study design aspects, and were recently discussed by Dou et al.^[21]

LTSL release their payload due to mild heating (≈ 41 °C) while still in the tumor microcirculation.^[22] The released drug will subsequently reach the cancer cells by free diffusion, and targeting does not rely on the EPR effect.^[23] This intravascular drug release approach (**Figure 1B**) offers the opportunity to achieve greater drug penetration, higher drug levels, and a more homogeneous distribution in tumor tissue compared with nonliposomal drug administration or other nanoparticle-mediated approaches that depend on the EPR effect.^[6] Shortcomings of LTSL are the usage of lysolipids and DSPE-PEG2000 acting as surfactants which compromise dispersion stability at 37 °C,^[24] the rapid exchange of lysolipids *in vivo*,^[25] and the induction of the formation of anti-PEG antibodies.^[26]

The aim of this study was to develop and preclinically evaluate a new long-circulating DOX-containing TSL formulation for the neoadjuvant treatment of locally advanced STS. Usage of lysolipids or PEGylated phospholipids was omitted, as a high stability in the presence of serum at 37 °C was one prerequisite for optimal TSL formulation.^[19] We systematically investigated the use of a well-defined, synthetic class of phospholipids (1,2-dipalmitoyl-*sn*-glycero-3-phosphatidyl-(oligo)-glycerols, DPPG_n, **Figure 1A**) as a component of TSL. This study is the first to

Prof. T. Knösel
Institute of Pathology
LMU Munich
Thalkirchner Str. 36, 80337 Munich, Germany

Dr. O. Schagon
Phospholipid Research Group
Max Planck Institute for Biophysical Chemistry
Am Faßberg 11, 37073 Göttingen, Germany

Prof. H. Gröll
University of Cologne
Faculty of Medicine
University Hospital of Cologne
Institute of Diagnostic and Interventional Radiology
Kerpener Str. 62, 50937 Cologne, Germany

Dr. M. Schmidt
Munich Cancer Registry
Institute for Medical Information Processing, Biometry, and Epidemiology
University of Munich
Marchioninstr. 15, 81377 Munich, Germany

Prof. A. M. Eggermont
Princess Máxima Center for Pediatric Oncology
University Medical Center Utrecht
Heidelberglaan 25, 3584 CS Utrecht, The Netherlands

Dr. T. L. ten Hagen
Department of Pathology
Laboratory Experimental Oncology and Nanomedicine Innovation Center
Erasmus (NICE)
Erasmus MC, 3015 CE Rotterdam, The Netherlands

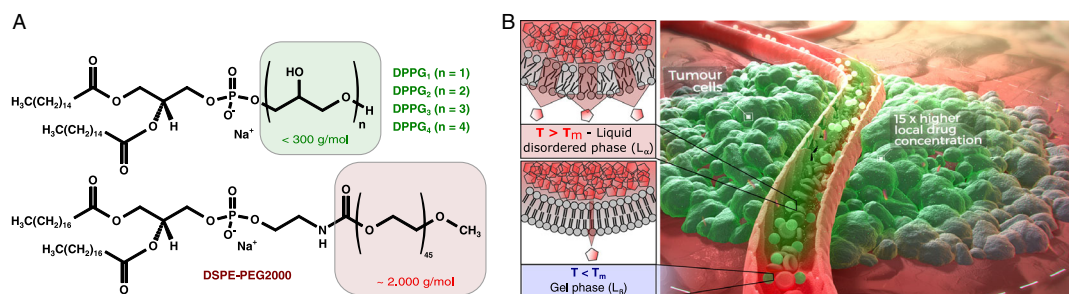


Figure 1. Drug-delivery mechanism and chemical structure of DPPG_n. A) Chemical structure of 1,2-dipalmitoyl-*sn*-glycero-3-phosphooligoglycerols in comparison with 1,2-distearoyl-*sn*-glycero-3-phosphoethanolamine-*N*-methoxy(PEG)-2000 (DSPE-PEG2000). B) Schematic representation of triggered intravascular drug delivery with TSL based on DPPG_n phospholipids. The membrane of TSL is stable at BT but becomes leaky around the phase-transition temperature (T_m) when the lipids melt from the solid-gel (L_β) to liquid-disordered phase state (L_α). The high local drug concentration of released DOX inside the blood vessel generates a gradient that pushes the drug into the tumor tissue. After cellular uptake, DOX accumulates in the nuclei of tumor cells.

describe the pharmacokinetic (PK), biodistribution (BD), and tumor-targeting capacity as well as therapeutic efficacy of this newly developed DPPG_n-based drug-delivery system in a rat sarcoma model, followed by a comparative oncology trial with spontaneously grown feline fibrosarcoma with positron emission tomography/magnetic resonance imaging (PET/MRI) and a histological response assessment. Our study demonstrates the potential of DPPG₂-TSL-DOX to strongly improve treatment outcomes for STS, but also as a general drug-delivery concept for treatment of solid tumors.

2. Results and Discussion

2.1. Synthesis of DPPG_n Phospholipids

1,2-Dipalmitoyl-*sn*-glycero-3-phosphoglycerol (DPPG₁), -diglycerol (DPPG₂), -triglycerol (DPPG₃), and -tetraglycerol (DPPG₄) were produced by organic synthesis under avoidance of enzymatic or polymerization reactions (Figure 2). The occurrence of mixed oligoglycerols in a lipid batch that might bias results in the present study was thereby excluded.

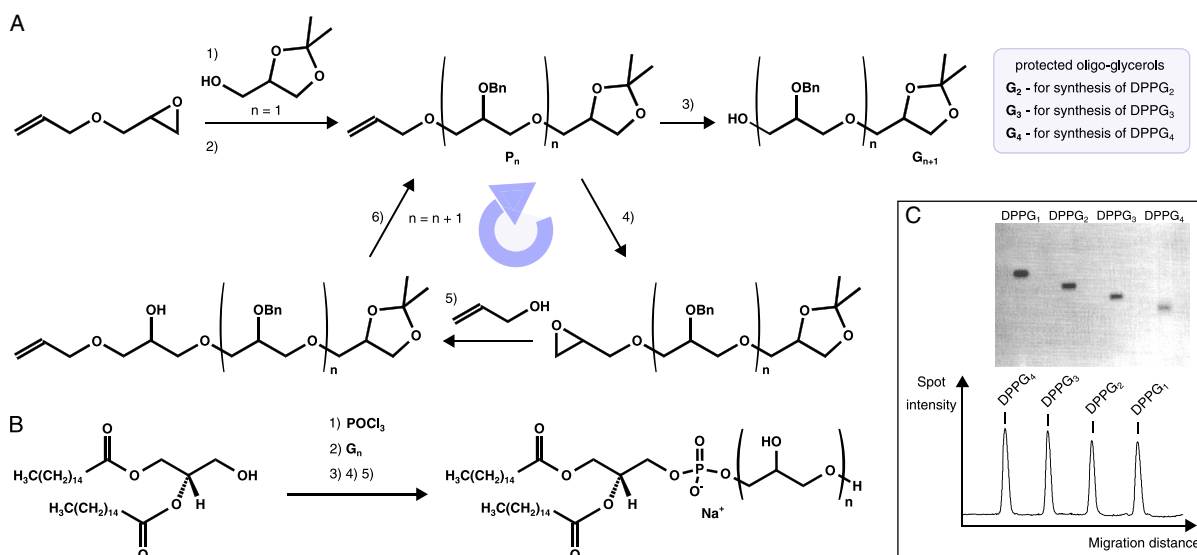


Figure 2. Synthetic scheme for DPPG_n and proof of purity. A) The protected oligoglycerols G₂, G₃, and G₄: G₂ is obtainable from commercially available allyl glycidyl ether in three reaction steps. P₁ is obtained by sodium hydroxide-catalyzed epoxide ring opening with excess isopropylidene glycerol (1) and benzylation of the resulting free secondary hydroxyl group (2). The allyl-protecting group is removed by basic rearrangement and acidic cleavage to result in G₂ (3). G₃ is obtained from P₁ by four additional reaction steps. P₁ is converted to P₂ by epoxidation (4), sodium hydroxide-catalyzed epoxide ring opening with excess allyl alcohol (5), and benzylation of the resulting hydroxide group (6). The allyl-protecting group in P₂ is removed as described earlier to result in G₃ (3). G₄ is obtained from P₂ with the same reaction steps as described for synthesis of G₃ from P₁. B) DPPG₂, DPPG₃, or DPPG₄ is obtained by phosphorylation with either G₂, G₃, or G₄ in five reaction steps, respectively. Reaction of POCl₃ with 1,2-dipalmitoyl-*sn*-glycerol in the presence of triethylamine results in 1,2-dipalmitoyl-*sn*-glycero-3-phosphodichloride, which is subsequently converted to the protected 1,2-dipalmitoyl-*sn*-glycero-3-phospho-oligo-glycerol-monochloride with the corresponding G₂, G₃, or G₄ at 35–40 °C, respectively (2). Afterward, hydrolysis with NaHCO₃ results in the formation of the sodium salt (3). The isopropylidene-protecting group is removed under acidic conditions (4), and the benzyl-protecting group is removed by catalytic hydrogenolysis (5). All reaction steps can be easily monitored by HPTLC. C) Discrimination and purity assessment of DPPG₁, DPPG₂, DPPG₃, and DPPG₄ with HPTLC.

2.2. PK Profile of DPPG_n-Based NTSL

Highly hydrated groups like PEG are capable of prolonging circulation half-life of liposomes.^[27] Our hypothesis was that oligomeric DPPG_n equipped with multiple hydroxyl groups rather forms lamellar structures in contrast to micelle-forming polymeric PEGylated lipids^[24] and will be similarly effective in

prolonging circulation half-life without negatively affecting dispersion stability. A clear beneficial effect on the liposome PK profile was observed when 10 mol% DPPG₂ or DPPG₃ was incorporated in DPPG_n-non-thermosensitive liposomes (NTSL) (**Figure 3A**). DPPG₂-NTSL and DPPG₃-NTSL showed a monoexponential decline of liposomal serum levels comparable with PEGylated liposomes^[27] with a prolonged circulation half-life of 17.6 ± 0.4 h and

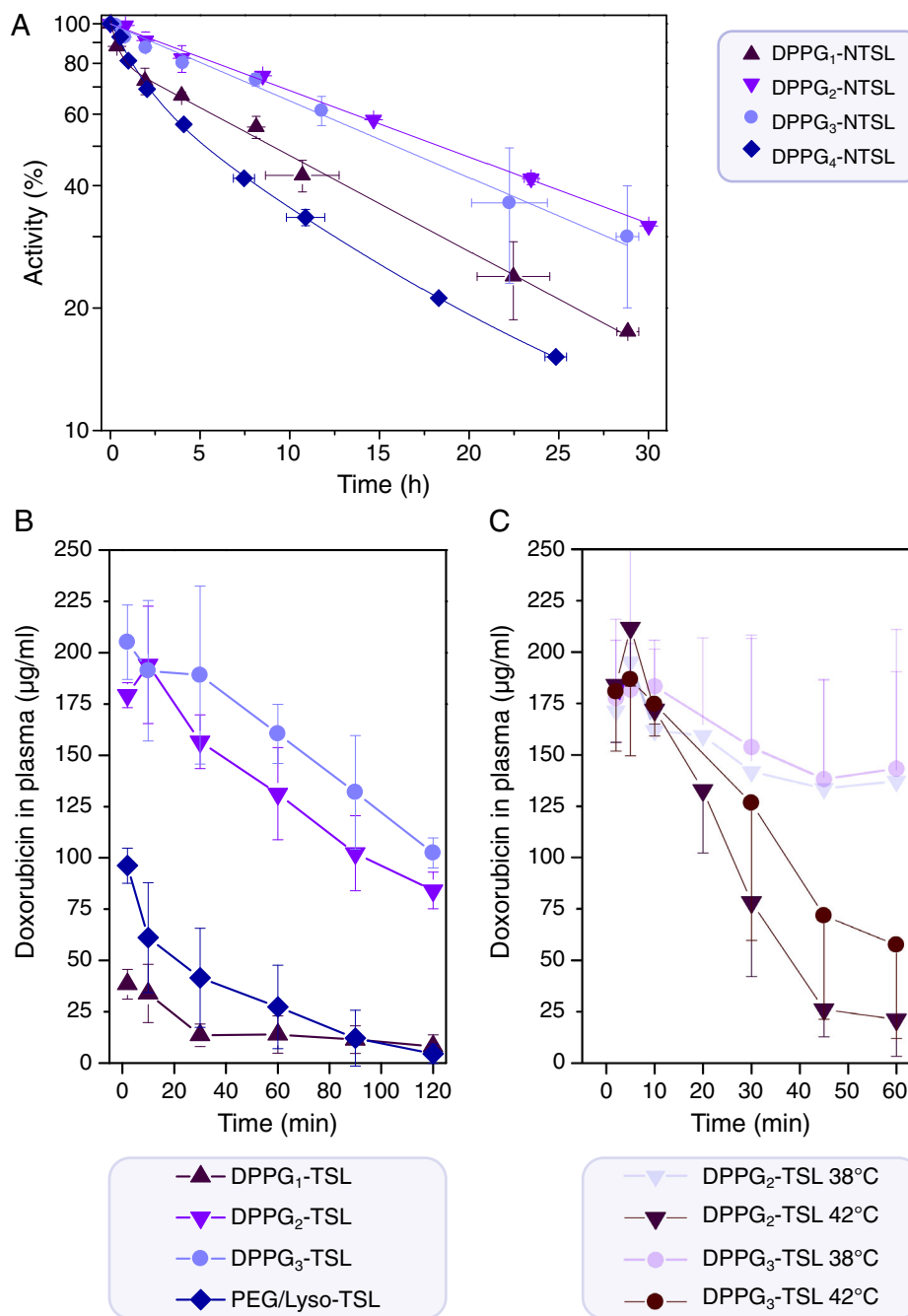


Figure 3. Effect of DPPG_n on PK of nanocarrier formulations in rats. A) PK profile of [³H]inulin incorporated in NTSL composed of DPPG_n/DPPC/cholesterol 1:4:5 (mol/mol) with $n=1-4$ after i.v. injection in male Wistar rats (100 µmol total lipid/kg body weight). Values expressed as average \pm S.D. of blood samples from three independent animals. B,C) PK profile in healthy rats of DOX formulated in distinct TSL formulations after i.v. application and treated with water bath RHT of one hind leg at 38 °C (B) and 42 °C (C), respectively. Calculated PK parameters are shown in Table S3, Supporting Information. The error bars represent standard deviation of three animals per group.

17.2 ± 2.6 h, respectively. Strikingly, NTSL with only one glycerol moiety less (DPPG₁) or one glycerol moiety more (DPPG₄) displayed rapid biexponential elimination from circulation, typical for nonsterically stabilized liposomes. DPPG₁-NTSL and DPPG₄-NTSL resulted in t_{α} of 0.4 h and 1.6 h, respectively. The terminal elimination (t_{β}) was 13.0 ± 0.5 h for both formulations. Prolonged circulation properties for DPPG₂- and DPPG₃-NTSL were dose independent between 25 and 100 μmol kg⁻¹ (total lipid concentration). It is obvious that steric hindrance of opsonization as discussed for PEGylated lipids^[27] is not the sole mechanism for prolonging circulation half-life. The smaller headgroups of DPPG₂ (74 Da) and DPPG₃ (148 Da) prolong circulation half-life of NTSL, whereas the effect is lost for DPPG₄ (222 Da).

2.3. In Vitro Properties of DPPG_n-Based TSL

Based on their advantageous PK profile when incorporated in NTSL, DPPG₂ and DPPG₃ were chosen for further investigation

in TSL formulations lacking cholesterol. DPPG₁ was used as a control. Lysolipids were omitted in DPPG_n-based TSL, as they led to impaired dispersion stability,^[28] resulting in relatively short blood circulation half-lives of the most advanced LTSL formulation.^[25] Lipid composition was DPPC/DSPC/DPPG_n with a molar ratio of 50:20:30 (DPPG_n-TSL), due to a favorable heat-triggered DOX release profile observed for DPPG₂-TSL.^[29] For the comparison of DPPG_n-TSL with a lysolipid-containing TSL formulation, DPPC/1-palmitoyl-*sn*-glycero-3-phosphocholine (P-Lyso-PC)/DSPE-PEG2000 90:10:4 (PEG/Lyso-TSL) was produced representing the initially published LTSL lipid composition.^[20] DOX was loaded with a high molar drug:lipid ratio of ≈0.15. The biophysical characteristics are summarized in Table S1, Supporting Information. Vesicle size was around 120 nm with narrow size distribution (polydispersity index, PDI < 0.16) for DPPG₂, DPPG₃, and PEG/Lyso-TSL, whereas DPPG₁-TSL had a vesicle size of ≈130 nm with a broader size distribution (PDI: ≈0.20). Cryo-transmission electron

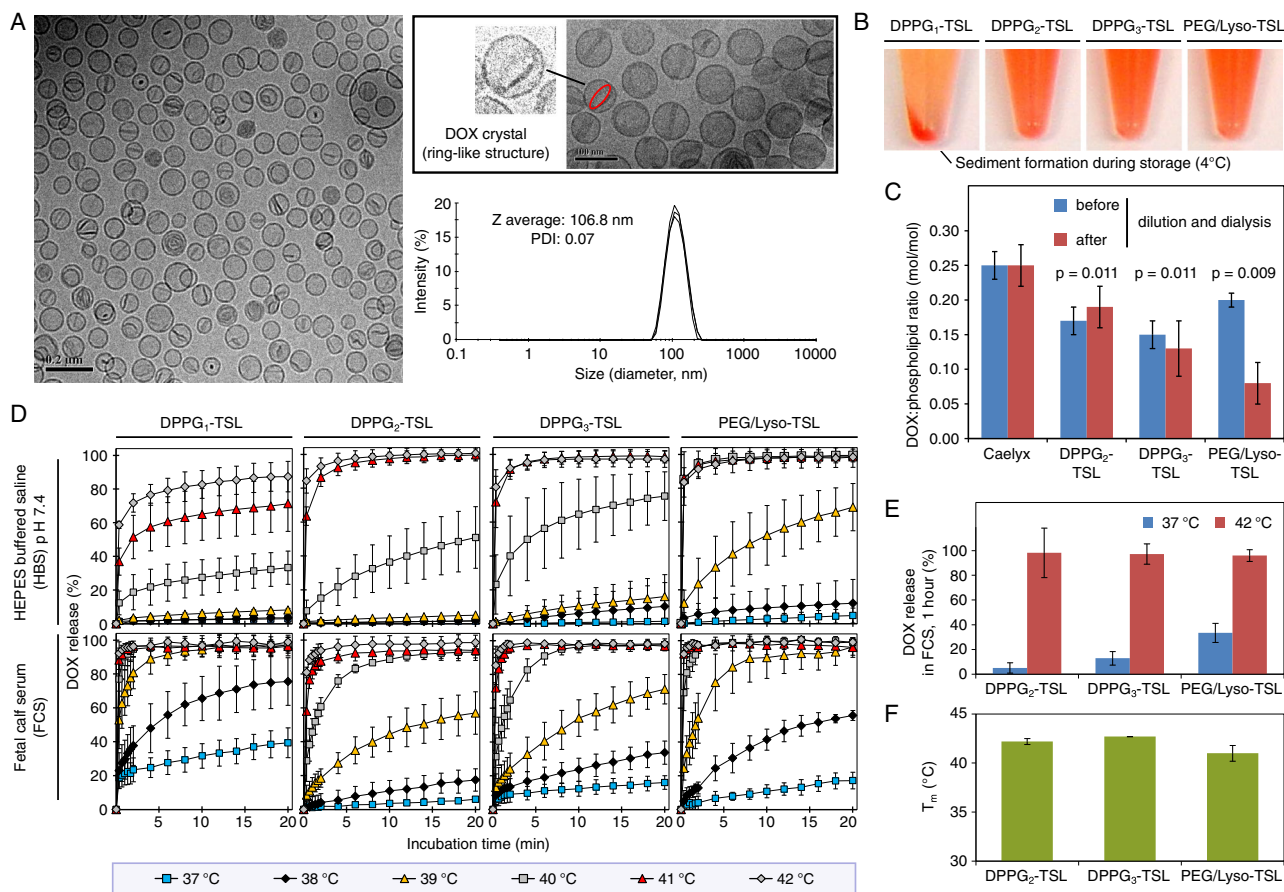


Figure 4. In vitro characterization of DPPG_n-TSL. A) Cryo-TEM images of two independently prepared DPPG₂-TSL batches showing spherical, unilamellar vesicles of well-defined vesicle size. DOX seems to form a ring-like crystal structure inside the vesicles (see inset). DLS data showed a vesicle size (z average) of 107 nm for both batches and a PDI of either 0.07 or 0.10, respectively. The molar drug:lipid ratio was 0.13 and 0.16, respectively. B) Images of polypropylene test tubes filled with different liposome suspensions after 12 h storage at 2–8 °C (total lipid concentration: ≈15 mM). C) Drug retention properties of distinct TSL formulations during rapid dilution. Subsequently, leaked DOX was removed by dialysis (over night, 2–8 °C, physiological saline). The DOX:phospholipid ratio of Caelyx is determined without the cholesterol content of the formulation. *P*-values are given for a paired *t*-test. D) Time-dependent DOX release profile from distinct TSL formulations in HEPES-buffered saline (HBS), pH 7.4, and fetal calf serum (FCS), respectively, measured with fluorescence spectroscopy. The standard error of the mean is shown. E) Temperature-dependent DOX release from distinct TSL formulations in FCS. F) Solid–gel-to-liquid-disordered phase-transition temperature (T_m) of distinct TSL formulations.

microscopy (TEM) of DPPG₂-TSL (Figure 4A) revealed spherical, unilamellar vesicles of well-defined vesicle size. DOX forms a ring-like crystal structure inside the vesicles, potentially originating from twisting hexagonally arranged fibers formed by stacked DOX molecules.^[30] DPPG₂-TSL and DPPG₃-TSL formed stable dispersions, whereas sedimentation during storage was seen for DPPG₁-TSL (Figure 4B). The increased robustness of the DPPG_{2/3}-TSL membrane bilayer compared with PEG-/Lyso-TSL was observed upon rapid dilution into physiological saline mimicking intravenous (i.v.) injection (Figure 4C). Incorporation of DPPG₂ and DPPG₃ into TSL strongly increased the release rate of DOX at 41 °C in buffer and serum (Figure 4D) by a factor of 4 compared with DPPG₁, yielding release rates comparable with PEG-/Lyso-TSL (Table S2, Supporting Information). This demonstrates that lysolipids are not necessary to achieve fast and complete payload release, as already shown with DPPG₂-TSL before.^[28] Stability of DPPG₂/DPPG₃-TSL at 37 °C in serum was superior to PEG-/Lyso-TSL (Figure 4E), indicating the positive effect of avoiding surfactants in the formulation. The main difference between DPPG₂/DPPG₃-TSL and PEG-/Lyso-TSL was the onset temperature for drug release, which was about 1 °C higher for the former ones (41 °C vs. 40 °C). This correlates with the solid–gel-to-liquid-disordered phase-transition temperature (T_m) of the formulations (Figure 4F).

2.4. PK Profile of DPPG_n-Based TSL in Rats

We have already shown that DPPG₂ yielded long circulating TSL with encapsulated carboxyfluorescein (CF)^[29] or gemcitabine,^[31] but have not yet applied formulations with actively loaded DOX which might affect blood stability or compared it with other formulations. Most notable were the differences in PK profiles of DOX in tested TSL formulations in healthy rats (Figure 3B, Table S3, Supporting Information). Similar to the DPPG_n-NTSL, DPPG₂/DPPG₃-TSL revealed a monoexponential decline with sustained systemic drug levels over a period of 60 min (>85% of maximum plasma peak concentration). PEG-/Lyso-TSL showed a more rapid biexponential DOX decline. DPPG₁-TSL failed to build sufficient plasma levels over time. The free hydroxyl groups of DPPG₂ and DPPG₃ might interfere with the binding of serum proteins to the liposome surface at 37 °C in a similar manner as shown for monoganglioside GM1.^[32] This might be facilitated by the strong binding of the serum protein apolipoprotein A1 on the surface of DPPG₂-TSL, which inhibits binding of other proteins.^[33]

To assess whether a substantial amount of payload can be released from the circulating nanocarriers in the heated area, DPPG₂/DPPG₃-TSL were injected i.v. in rats where the whole hind leg was heated to a temperature of 41 °C in a water bath, whereas the core body temperature (BT) was maintained at 38 °C. Under these conditions, where less than 5% of the body volume was heated, ≈55–70% of the injected dose was released within this confined compartment in a period of 60 min, resulting in a more rapid depletion of DOX from the circulation (Figure 3C).

Repeated injection of PEGylated nanoparticles can negatively affect the circulation half-life of such systems.^[26] Applying a second dose of DPPG₂-TSL to healthy rats 7 or 14 days after the first

application had no effect on the clearance of DOX (Figure S3, Supporting Information).

2.5. Visualization of DPPG_n-Based TSL Characteristics Using Intravital Fluorescence Microscopy

The principle of intravascular drug release was tested with dual-fluorescently labeled DPPG₂-TSL, demonstrating almost no extravasation within 90 min, favorable vesicle stability, and heat-triggerable drug release even after 60 min (Figure 5A).

When equal quantities of DOX loaded into TSL were administered and reached the window chamber heated to 41 °C, DPPG₂- and DPPG₃-TSL resulted in higher and more homogeneous DOX-tissue fluorescence compared with PEG-/Lyso-TSL, where the DOX signal was restricted to areas near blood vessels (Figure 5B). DOX uptake was mainly nuclear. Time-dependent tissue DOX uptake was quantitatively assessed by measuring the fluorescence intensity of the whole image during 60 min of heating (Figure 5C). All tested TSL showed a comparable initial fluorescence profile with a steady increase of DOX tissue uptake over time. For PEG-/Lyso-TSL, this leveled off and declined within 20 min after administration, but continued for DPPG₂-TSL until 60 min, and for DPPG₃-TSL until the end of the experiment at 120 min. This difference is mainly explained by the improved PK profile of DPPG_{2/3}-TSL (Figure 3B), resulting in sustained high intravascular DOX concentrations inside the heated tissue, with consecutive greater tissue penetration.^[6]

2.6. BD and Antitumor Efficacy of DPPG_n-Based TSL in a Rat Sarcoma Model

DPPG₂ can be incorporated up to 70 mol% into TSL, and 30 mol% has been found optimal for release at 41 °C in vitro.^[29] This amount was confirmed in rat experiments, where DOX tumor uptake was measured for TSL differing in DPPG₂ content (Figure S1, Supporting Information). While PK profiles were almost similar, DOX-tumor uptake for 20 and 30 mol% DPPG₂-TSL was significantly higher as compared with 10 mol% DPPG₂-TSL. This is most probably due to the faster heat-triggered drug release with higher DPPG₂ content in the TSL formulation.^[29]

DOX tumor uptake of several formulations was investigated in a subcutaneous rat sarcoma model (BN 175). At a dose of 5 mg kg⁻¹, DOX tumor concentration after 60 min of RHT at 41 °C for DPPG_{2/3}-TSL was increased tenfold compared with the nonheated tumor and was significantly higher than with conventional DOX or PEG-/Lyso-TSL (Figure 6A). The DOX concentration in the unheated tumors was <10% compared with the heated tumors. As DOX uptake in the nonheated tumor is influenced by recirculating DOX released at the heated tumor,^[34] the true difference might be even larger. The maximum DOX concentration achieved in the tumor for PEG-/Lyso-TSL was threefold lower than that obtained for DPPG₂/DPPG₃-TSL. For conventional DOX, the tumor tissue concentration in the heated tumors increased twofold upon RHT and reached similar drug levels as obtained with the PEG-/Lyso-TSL. Caelyx achieved the highest maximum drug levels after 24 h. Liposome uptake to

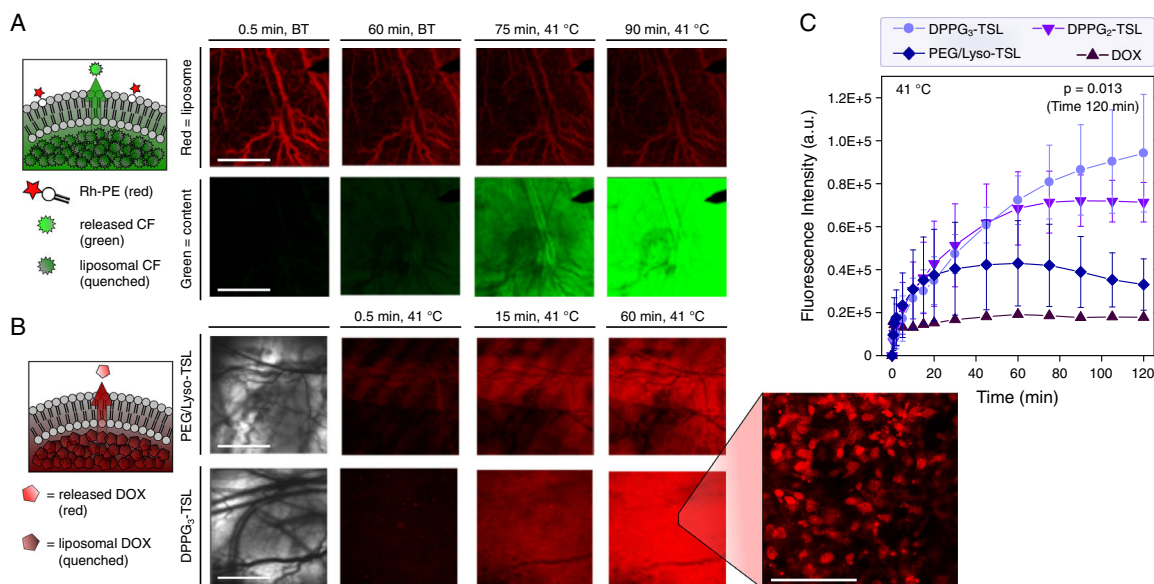


Figure 5. In vivo confocal imaging of dorsal skinfold window chambers in rats lacking tumor grafts showing long-circulating properties of DPPG_{2,3}-TSL. A) Representative fluorescence images after i.v. administration of DPPG₂-TSL labeled with RhPE and loaded with CF at quenching concentration. During 90 min of sequential imaging most of the TSLs remained intravascularly, and unspecific CF release was negligible at BT during the first 60 min. However, after subsequent heating of the skinfold chamber to 41 °C, a bright green fluorescence signal appeared outside the blood vessels, indicating intravascular CF release from circulating TSL followed by rapid diffusion into the surrounding tissues. White bar = 2 mm. B) Exemplary fluorescence images after i.v. administration of DPPG₃-TSL and PEG-/Lyso-TSL loaded with DOX. The chambers were preheated at 41 °C for 5 min before administration. Images were obtained after 0.5 min, 15 min, and 60 min. Corresponding bright-field images are given as first image in each row (bar = 2 mm). Images for DPPG₂-TSL are not shown because they are not significantly different from DPPG₃-TSL. High magnification of skin tissue after DPPG₃-TSL application and 60 min heating at 41 °C, demonstrating nuclear uptake of DOX (bar = 100 μm). C) Time-dependent skin DOX fluorescence after i.v. application of distinct TSL formulations with encapsulated DOX (DPPG₂-TSL, DPPG₃-TSL, PEG-/Lyso-TSL) or conventional DOX and simultaneous heating to 41 °C. The error bars represent standard deviation of three animals per group. Multiple regression analysis between treatment groups was conducted for the time point of 120 min ($p = 0.013$).

tumors was increased by RHT (Figure 6A) as shown previously.^[35,36]

DOX uptake in the heart muscle was the highest upon conventional DOX treatment and virtually similar to those obtained upon PEG-/Lyso-TSL. DOX uptake with DPPG_{2/3}-TSL was 40% lower ($p < 0.02$) (Figure 6B).

BN 175 sarcoma tumors were rapidly growing, and control rats treated with saline 0.9% i.v. and RHT had to be euthanized within 5–7 days (Figure S2, Supporting Information). 5 mg kg⁻¹ conventional DOX or Caelyx, both combined with RHT, had only a minor effect on tumor growth. Interestingly, Caelyx reached comparable high DOX-tumor levels as DPPG_{2/3}-TSL (Figure 6A) but with a similar low efficacy as conventional DOX in the therapeutic studies (Figure S3, Supporting Information). Presumably, most of the DOX remains in the liposomal carrier and is not bioavailable.^[17] All rats had to be euthanized before day 10. The situation was different for DPPG₂-/DPPG₃-TSL in combination with RHT, where both formulations led to complete tumor regressions (DPPG₂-TSL: 3/6, DPPG₃-TSL: 4/6). Unfortunately, the treatment effect was accompanied with considerable foot skin toxicity leading to swelling, redness (Figure S2, Supporting Information), and finally to ulcerations of the feet. As this was not seen for PEG-/Lyso-TSL or Caelyx with RHT, this effect is clearly attributed to the high local DOX levels in the foot pad for the DPPG₂-/DPPG₃-TSL if the whole leg is

heated. This off-site toxicity was completely abolished, when a more focused heating method using an adjustable light source was used. Tumor DOX-uptake factors vary depending on tumor size and heating method^[37] and can be increased up to 17-fold by applying a more focused heating method (lamp) in the same tumor model.^[37] Here, with a 2.5-fold lesser dose (2 mg kg⁻¹) administered with DPPG₃-TSL, remarkable tumor growth delays and several complete tumor regressions (3/6) were achieved. For PEG-/Lyso-TSL, only 1/6 animals showed delayed tumor growth. Analysis of overall survival (Figure 6C) demonstrated no difference between 0.9% saline, conventional DOX, and Caelyx (5 mg kg⁻¹) but a significant advantage for DPPG₃-TSL over PEG-/Lyso-TSL at a much lower dose of 2 mg kg⁻¹ ($p = 0.002$).

2.7. Therapeutic Efficacy of DPPG₂-TSL-DOX in Cats with Spontaneous Fibrosarcoma

We followed the comparative oncology approach and treated spontaneous feline fibrosarcoma (Figure 7A) in the neoadjuvant setting with DPPG_n-based TSL, as rat models are usually limited in clinical translation.^[38] These naturally occurring tumors grow invasively and show clinical and biological similarities to human STS^[39] and are therefore more representative. This is also true regarding nanoparticle-mediated drug uptake, as EPR is generally overrepresented in subcutaneous tumor models.^[40]

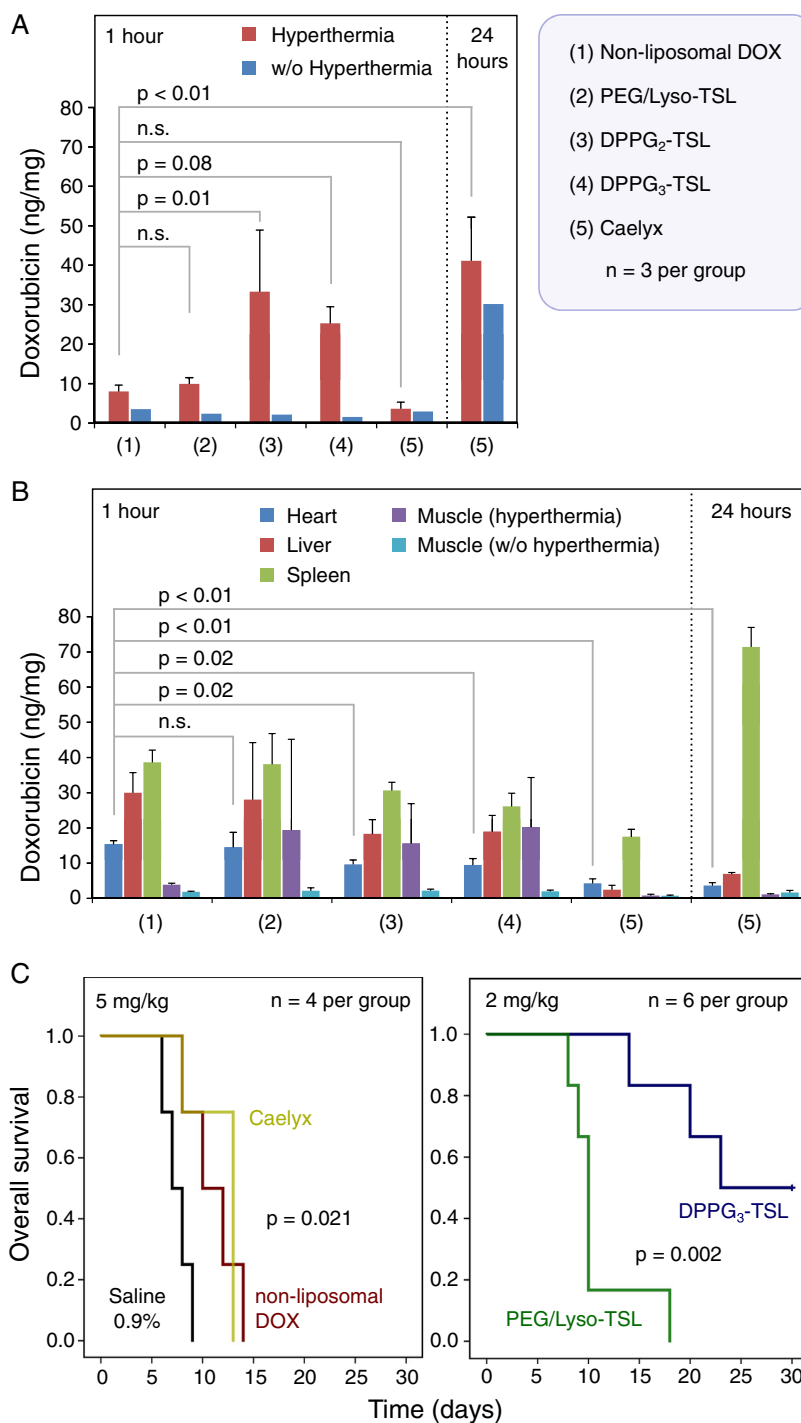


Figure 6. In vivo measurement of tumor DOX uptake, organ distribution, and overall survival in the BN175 rat sarcoma model. A) Tumors were implanted in both hind legs. The experiment was started when one of the tumors reached a volume of $\approx 500 \text{ mm}^3$. The tumor-bearing hind leg was then heated in a water bath and different DOX-containing TSL formulations, conventional DOX or Caelyx were i.v. administered at a dose of 5 mg kg^{-1} DOX equivalent when the tumor temperature reached 41°C ($n = 3$). After 60 min of heating, animals were euthanized and tumor DOX uptake was measured. For Caelyx, additional measurements 23 h after the end of heating were carried out. B) DOX uptake in heart, liver, spleen, muscle of the heated hind leg and muscle of the unheated hind leg was determined from the same rats at identical time points. The error bars represent standard error of the mean. *P*-values are obtained by multiple regression techniques. C) For efficacy studies tumors were implanted in one of the hind legs. Treatments were started when the tumor reached $\approx 100 \text{ mm}^3$ in size. Conventional DOX or different liposomal DOX formulations were i.v. administered when the tumor temperature reached 41°C ($N = 6$). Heating was conducted over a period of 60 min. Tumor growth was subsequently measured until animals reached predefined endpoint criteria for euthanasia (tumor size $> 20 \text{ mm}$ in diameter or ulceration). Kaplan–Meier survival plots are shown for all tumor-bearing rats. *P*-values are given from log rank tests.

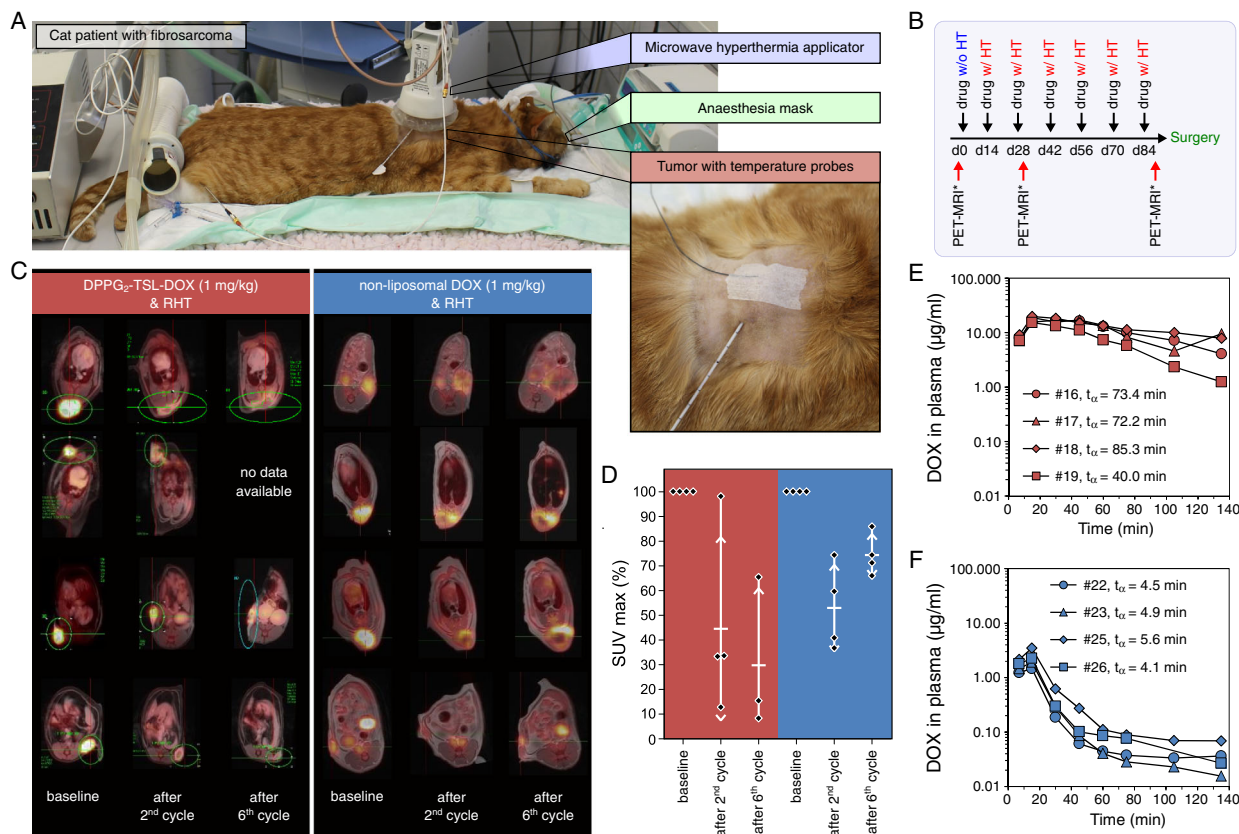


Figure 7. Neoadjuvant treatment of feline sarcoma with DPPG₂-TSL-DOX + RHT and conventional DOX + HT. A) Cat patient with spontaneous STS located at the back. Inset shows the location of the temperature probes. Microwave hyperthermia (tumor target temperature: 41.5 °C) was applied for 60 min under general anesthesia. B) Study outline. Routine rechecks (general examination, complete blood count, blood chemistry, tumor measuring) seven days before and after each treatment. C) Subsequent FDG-PET/MRI fusion images at baseline, after two and after six cycles of therapy at the dose of 1 mg kg⁻¹ DOX, and D) High–low plot illustrates metabolic response of individual animals. E) PK profile of DOX encapsulated in DPPG₂-TSL in cats treated with 1 mg kg⁻¹ DOX without RHT. F) PK profile of conventional DOX in cats treated with 1 mg kg⁻¹ DOX without RHT. Calculated PK parameters are shown in Table S6, Supporting Information.

Conventional DOX is the best-known standard for treatment of feline fibrosarcomas, with response rates in the range of 40% for DOX and Caelyx (1 mg kg⁻¹).^[41]

Due to the less complex synthesis of DPPG₂ and similar in vitro and in vivo behavior compared with DPPG₃, we decided to continue our development program with DPPG₂-TSL-DOX compared with conventional DOX.

Analogous to the clinical situation encountered in human STS patients, we used a clinically used radiofrequency applicator for RHT and used PET/MRI to assess the metabolic tumor response. FDG PET/MRI imaging was used for response assessment, as it is clinically the most sensitive biomarker for response in neoadjuvant treatment protocols.^[42]

In a preceding study,^[43] treatment of cats with DPPG₂-TSL-DOX at a dose level of up to 0.6 mg kg⁻¹ DOX could be regarded as safe, including two metabolic responses, and allowed for subsequent surgery in four cats. Now, we followed the concept of neoadjuvant chemotherapy plus RHT in cats with locally advanced but resectable tumors. The dosage was escalated to 0.8 mg kg⁻¹ DOX. Three cats treated with DPPG₂-TSL-DOX did not show dose-limiting toxicity but already showed

impressive metabolic responses with partially cystic transformation of the tumors (Table 1).

In the last dose cohort with 1.0 mg kg⁻¹ DOX, four cats each were treated with DPPG₂-TSL-DOX (TSL group) and four with conventional DOX (control group) (Table S4, Supporting Information). Median tumor temperatures were ≈41.9 °C (Table 1). Three of four cats in the TSL group received all six cycles, whereas 1/4 cat had to stop treatment after the third cycle due to cardiac arrhythmias. Three out of four cats in the control group received six cycles of DOX, whereas 1/4 cat had to stop after the fifth cycle due to excessive weight loss. Tumor resection was conducted in all cats that received DPPG₂-TSL-DOX and in 3/4 cats in the control group at the end of treatment. One out of four cats of the control group developed lung metastases during therapy and was therefore not operated. There was no grade 3–4 hematologic, liver, or kidney toxicity detectable in the blood analytics for both groups (Table S5, Supporting Information).

PK evaluation revealed a notable different DOX elimination between the two groups (Table S6, Supporting Information and Figure 7). DOX half-life without RHT, DOX plasma concentration at the end of infusion, and AUC_{1–135 min} (AUC, area

Table 1. Summary of intratumoral temperatures and response data in cats (MRI: RECIST response, FDG-PET: PERCIST response, Pathologic assessment of resected tumor: % of vital tumor cells).

Cat ^{a)}	DOX dosage [mg kg ⁻¹]	Intratumoral temperatures					CEM43	Tumor response after six cycles		
		T _{mean} [°C]	T ₉₀ [°C]	T ₅₀ [°C]	T _{max} [°C]	T _{min} [°C]		RECIST	PERCIST [SUV _{max}]	Vital tumor cells [%]
TSL group (DPPG ₂ -TSL-DOX):										
# 13	0.8	43.7	41.9	44.6	46.2	37.7	867.7 ^{b)}	N/D	N/D	
# 14	0.8	41.8	41.4	41.9	43.1	39.7	80.3	SD	SD	
# 15	0.8	41.9	41.8	42.0	43.2	39.3	61.7	PD	N/D	
# 16	1.0	41.8	41.6	41.9	42.7	38.5	80.4	SD	PR	<5
# 17	1.0	41.9	41.9	41.9	42.8	39.3	42.2	SD	PR	5–10
# 18	1.0	41.9	41.8	42.0	42.5	38.8	83.2	PD	PR	<5
# 19	1.0	41.9	41.6	42.0	42.7	39.7	77.7	SD	PR	10–20
Control group (conventional DOX):										
# 22	1.0	41.9	41.8	41.9	42.8	40.7	82.1	PD	SD	50–60
# 23	1.0	41.9	41.7	41.9	43.6	40.1	81.3	PD	SD	No specimen ^{c)}
# 25	1.0	41.9	41.8	41.9	42.9	39.5	70.0	SD	PR	70–80
# 26	1.0	41.9	41.8	41.9	42.5	39.7	82.5	SD	SD	>95

^{a)}Response Evaluation Criteria in Solid Tumors (RECIST): Response was calculated from longest diameters determined in MRI; PR: $\geq 30\%$ decrease from baseline; PD $\geq 20\%$ increase from baseline; SD: neither PR or PD criteria met. Positron Emission Tomography Response Criteria In Solid Tumors (PERCIST): PR: metabolic partial response ($\geq 30\%$ decrease in SUV_{max}); SD: metabolic stable disease ($<30\%$ decrease and $<30\%$ increase in SUV_{max}). CEM43: Cumulative equivalent minutes at 43 °C. N/D: Not done. Note: #15 received only four treatments due to tumor abscess formation, most likely related to catheter implantation; #17 received only four treatments due to cardiac arrhythmias; and #25 had to stop after five treatments due to excessive weight loss. ^{b)}Target temperature was 45 °C; thus, thermal dose was considerably higher, indicated also by the median temperature of 44.6 °C. The unpaired *t*-test did not show a significant difference between main intratumoral temperatures (T_{mean}, T₅₀, T₉₀, T_{max}, CEM43) and group (DPPG₂-TSL-DOX 1.0 mg kg⁻¹, conventional DOX 1.0 mg kg⁻¹) with the exception of T_{min} (*p* = 0.049). ^{c)}No surgery was conducted due to PD with lung metastases in the third PET–MRI.

under the curve) was 13.3-fold higher, 6.6-fold higher, and 24.4-fold higher for cats in the TSL group compared with the control group, respectively. With RHT, cats receiving DPPG₂-TSL-DOX showed a tendency for faster clearance from plasma (*t_w*, Table S6, Supporting Information), indicating heat-triggered DOX release in tumor tissue, but the effect of RHT was less pronounced than in lower-dosage levels,^[43] as the heated tumor volume was small compared with the overall body volume.

All cats treated with DPPG₂-TSL-DOX achieved metabolic partial response (mPR, $>30\%$ decrease in SUV_{max}) either after two cycles (4/4) or after six cycles (3/4, one dropout). For cats treated with conventional DOX, a mPR was only achieved after two cycles (4/4). Notably, all cats treated in the control group showed metabolic progression after six cycles of treatment (4/4) (Table 1 and Figure 7). Radiographic response showed stable disease (SD) in 3/4 cats and progressive disease (PD) in 1/4 cats treated for six cycles with DPPG₂-TSL-DOX (Table 1). Cats treated with conventional DOX showed SD (2/4) and PD (2/4), respectively. Histopathologic response assessment (Table 1) revealed all cats in the TSL group with ≤ 10 –20% residual vital tumor cells. For the control group, all accessible cats showed ≥ 50 –60% residual vital tumor cells (one dropout, metastatic disease). The change in response pattern (sustained tumor response vs. early progression) suggests that drug resistance mechanisms based on limited intratumoral drug distribution^[44] might be overcome by the more effective drug delivery using DPPG₂-TSL-DOX.

3. Conclusion

While ATC-based neoadjuvant chemotherapy and RHT provide improved survival for patients with locally advanced high-risk STS, tumor downsizing in most patients is insufficient, and there is a strong rationale for improving drug delivery. We can show that a new class of TSLs can be obtained using DPPG₂ as excipient, offering improved stability at BT, fast release kinetics, and therefore improved plasma concentration over the RHT period. Convincing stability at physiologic conditions combined with high antitumor activity in a rat sarcoma model can be transferred (after a precedent dose-finding study) into a two-arm comparative oncology trial in feline sarcoma. After six cycles of neoadjuvant treatment, all cats treated with DPPG₂-TSL-DOX + RHT showed an mPR confirmed by a good histopathologic response, whereas cats treated with conventional DOX + RHT started to progress after the initial two cycles of therapy. Based on these data, DPPG₂-TSL-DOX might be suitable for improving the outcome of patients with locally advanced STS in the neoadjuvant setting. Further clinical development of DPPG₂-TSL-DOX is ongoing.

4. Experimental Section

Materials: Lipids were from Corden Pharma (Liestal, Switzerland), except DSPE-PEG2000 (Avanti Polar Lipids, Alabaster, USA), 1,2-dipalmitoyl-*sn*-glycero-3-phosphoethanolamine-*N*-(lissamine rhodamine B sulfonyl) (RhPE, Avanti Polar Lipids), and cholesterol (Fluka, Buchs,

Switzerland). DOX was purchased from Sigma Aldrich (Munich, Germany) and [³H]-Inulin from Amersham-Buchler (Braunschweig, Germany). All other chemicals were from Carl Roth (Karlsruhe Germany) or Sigma Aldrich (Munich, Germany). Aqueous solutions were prepared with ultra-pure water (Milli Q Advantage, Millipore).

Synthesis of DPPG_n Phospholipids: DPPG_n were synthesized as described in detail in another study (WO97/30058). Purity was judged by HPTLC (silica gel). Chloroform/methanol/acetic acid/water, 100:60:20:5 (vol/vol), followed by chloroform/methanol, 20:1 (vol/vol), were applied as eluents. Staining was done with phosphoric acid/CuSO₄ solution.

Preparation of NTSL Formulations: DPPG_n/DPPC/cholesterol, 1:4:5 (mol/mol) (DPPG_n-NTSL), were prepared by dissolving the lipids in 2-propanol and subsequent removing in a rotary evaporator. The lipid film was dried under vacuum. Hydration was conducted with 0.9% saline (60–65 °C, 45 min). Small unilamellar vesicles were formed by sonication (Branson Sonic Power sonifier with titanium tip). After centrifugation, the dispersion was incubated with [³H]-inulin (0.2 mCi mL⁻¹, 0.9% saline) in an ultrasonic bath (50 °C, 30 min). Non-liposomal [³H]-inulin was removed by chromatography.

Preparation and Characterization of TSL Formulations: Formulations with encapsulated DOX were prepared and characterized as published in other studies.^[28] Quality of batches prepared for the treatment of feline fibrosarcoma was controlled with measures described in the study by Zimmermann et al.^[43] Only batches within the predefined acceptance criteria were applied to patient cats.

Cryo-TEM: Cryo-TEM was conducted in a low-dose mode using a Gatan cryoholder operating at -170 °C and an FEI Titan Krios TEM equipped with a field-emission gun (FEG) operating at 300 kV. Images were recorded using a 2 k × 2 k Gatan charge-coupled device camera equipped with a postcolumn Gatan energy filter (GIF) at an angle of 08. The sample vitrification procedure was conducted using an automated vitrification robot, viz., FEI Vitrobot Mark III. The Quantifoil grids were made hydrophilic with surface plasma treatment using a Cressington 208 carbon coater operating at 5 mA for 40 s prior to the sample preparation and vitrification.

Quantification of DOX in Plasma and Tissue Samples: DOX concentration was quantified by high-performance liquid chromatography.^[37]

Animal Studies: Studies were conducted on male Wistar and male Brown Norway rats (Charles River Laboratories) with protocols approved by the respective Institutional Animal Care and Use Committees (AZ: 55.2-1-54-2532-144-2011).

PK studies with NTSL: About 24 h prior to injection of NTSL, permanently indwelling fine polyethylene catheters (PE10, inner diameter: 0.28 mm) were implanted into the right jugular vein under general anesthesia. Studies were conducted in awake Wistar rats (250–350 g) with blood drawings after defined time points. Before scintillation counting (LS 6000, Beckman), whole blood samples were combusted using an OX-300 Biological Oxidizer (R.J. Harvey Instrument).

Rat STS Animal Model: BN175 cells were cultured at 37 °C in a humidified atmosphere of 95% air and 5% CO₂.^[31] Brown Norway rats (250–350 g) were used.

PK measurements: Injections were conducted via the dorsal vein of the penis. Blood was collected via repeated tail vein bleedings (Multivette 600 LH, Sarstedt). The rats were kept under anesthesia for the first 30 min. Recovery from anesthesia was allowed between further time points. For measurements during RHT, one hind leg was placed in a 42 °C water bath for 1 h, yielding a temperature of 41 °C.

BD studies: Animals with subcutaneously implanted sarcomas (BN175) grown to a size of 499 ± 156 mm³ on both hind legs have been used. One tumor-bearing leg was placed in a 42 °C water bath for 1 h. Heating started 10 min before drug injection. Animals were euthanized immediately after the end of RHT treatment and intravenously infused with saline 0.9% using a peristaltic perfusion pump before harvesting of tumors, neighboring muscle tissue from both hind legs, heart, liver, and spleen. For Caelyx, additional blood and tissue sampling 23 h after the end of RHT treatment was conducted. Samples were immediately cooled on ice. Plasma was generated by centrifugation (10 min,

2000 g). Plasma and tissue samples were stored at -20 °C and -80 °C until further processing, respectively.

Antitumor efficiency: Treatment (5 mg kg⁻¹ DOX) was conducted as described earlier but with smaller tumors (≈120 mm³) grown only in one hind leg. In rats treated with 2 mg kg⁻¹, RHT was applied by a cold light source and temperatures were controlled with intratumoral catheters.^[31] The target tumor temperature for all groups was 41.0 °C. Animals were weighed, and tumor sizes were measured every other day. Tumor volume was calculated (volume = length × width × height × π/6). Animals were followed until a tumor diameter >20 mm was reached or if the tumor became ulcerated or necrotic. Maximum observation time was 30 days post-treatment. Relative tumor volumes at day *n* were calculated: V(*n*)/V₀, where V₀ is the tumor volume at day of treatment.

Dorsal Window Chamber Model: Brown Norway rats (100–165 g) with dorsal window chambers were anesthetized with isoflurane and positioned on a custom-designed microscope stage. An external circular resistive electric heating coil attached to the back side of a glass coverslip provided homogenous temperatures of 41.0 ± 0.3 °C measured with thermocouples (H. Drijfhout & Zoon's edelmetaalbedrijven, Amsterdam). Core BT was maintained with a warming pad (37 °C). Polyethylene catheters implanted into the right jugular vein were used for injection. Background images were captured before injection. Fluorescent dyes were monitored by an appropriate laser. Images of transmission channels and fluorescent channels (×2 objective lens) were recorded at defined time points. Images (512 × 512 pixels) were analyzed with a Zeiss image program (LSM, Germany). DOX uptake was quantified as average intensity per field of view at 150–255 threshold by Image J (National Institutes of Health, USA).

Animal Studies in Cats with Spontaneous Fibrosarcoma: The study was conducted as reported previously.^[43] In brief, privately owned cats with histologically confirmed STS were enrolled (Table S4, Supporting Information). The treatment protocol was approved by the governmental department (AZ: 55.2-1-54-2531-1-08) and is shown in Figure 7B. All groups obtained simultaneous RHT (41.5 °C as target temperature, 60 min, BSD 50 microwave generator, MA-151 applicator, Sennewald Medizintechnik, Munich, Germany). Preservation of the skin above the tumor was provided by a circulating deionized water-cooling system. DOX formulations were infused intravenously (15 min) after an intratumoral temperature of 41.5 °C was achieved. BT was measured by additional rectal and esophageal thermometry probes. One invasive Bormann sensor controlled the intratumoral temperature and another noninvasive one on the surface of the skin. The invasive thermometer was moved manually along the catheter track and temperatures were recorded every minute to measure a temperature profile across the catheter path. Tumor heating was tried to be maintained at a steady state as the power heating the tumor tissue was adapted automatically to the recorded temperature.

PET/MR Imaging: A simultaneous hybrid device for whole-body imaging was used, with a 3.0 Tesla MRI and avalanche photodiode-PET detector technology (Biograph mMR, Siemens, Erlangen, Germany). The cats were imaged 107 ± 22 min after i.v. injection of 55.6 ± 11.3 MBq [¹⁸F]-fluorodeoxyglucose. One bed position with an emission time of 10 min was used to cover the body stem with the tumor of the animals. Images were reconstructed using an ordered-subset expectation maximization (OSEM 3D) iterative reconstruction algorithm (3 iterations, 21 subsets) and were corrected for scatter and attenuation. Image analysis was conducted on a dedicated workstation and software (Syngo MMWP and Syngo TrueD, Siemens Medical Solutions, Erlangen, Germany). For quantitative analysis of the PET data, standardized uptake value (SUV)-based analysis of tracer uptake in the tumors was conducted. Volumes of interest (VOIs) were placed over matching corresponding FDG images of the tumor lesions. To calculate SUV_{max} for tumor lesions, the axial slice with the maximum SUV of the lesion was first located automatically, using standardized software for images of both scanners, and then a 1.5 cm region of interest was drawn around the hottest pixel. An isocontour VOI including all voxels above 20% and 50% of the maximum was then created to calculate mean SUVs. Within all VOIs, mean and maximum SUVs were measured. Evaluation of response was conducted by

measures of the longest tumor diameter with MRI according to RECIST and determination of SUV_{max} according to the PERCIST criteria.

After intravenous catheter placement, the cats were premedicated with butorphanol (0.2 mg kg⁻¹ intravenously, Vetergesic; 10 mg ml⁻¹). For the PET/MR imaging, general anesthesia was induced using propofol (4–6 mg kg⁻¹ intravenously; Narcofol; 10 mg kg⁻¹), intratracheal intubation and artificial ventilation was conducted, while anesthesia was maintained with inhalation of isoflurane. Monitoring of heart rate (HR), end-tidal CO₂ (PE'CO₂), and arterial oxygen saturation (SpO₂) were conducted during anesthesia.

Microscopical Analysis: Formalin-fixed paraffin-embedded (FFPE) tumor tissues were cut into 3 μm sections, and H&E staining was conducted (standard procedures, Institute of Pathology, University of Munich).

Statistical Methods: Results were illustrated as means ± standard deviation of at least three independent experiments. An independent *t*-test was used for two group comparisons, whereas a dependent *t*-test compared pre–post outcomes. Time-to-event data were analyzed by the Kaplan–Meier method. Differences in survival estimates were assessed by a log-rank test. High–low plots were used for demonstration of metabolic responses. Multiple linear regression models with repeated measurements and mixed effect design were fitted to the data to determine the extent to which parameters can explain multilevel effects. All statistical procedures were conducted using an exploratory approach, and the maximum type I error probability associated with all statistical tests in the analyses was 0.05. SAS Software 9.4 (SAS Institute Inc., Cary, USA) was utilized.

Supporting Information

Supporting Information is available from the Wiley Online Library or from the author.

Acknowledgements

This work is dedicated to Professor Hansjörg Eibl, Ph.D. (Max Planck Institute for Biophysical Chemistry), who invented the DPPG₂ technology and inspired generations of scientists with his outstanding passion for phospholipids and their application in nanomedicine. With deep gratitude the authors highlight Gerben Koning's Ph.D. contribution and his support. The authors thank Anja Zengerle, Kirsten Wachholz, Lisa Pointner, Angela Knauerhase at the LMU Munich, Sylvia Schachoff, Claudia Meisinger, Anna Winter at the Klinikum Rechts der Isar, and Debby Schipper at the Erasmus Medical Center, Rotterdam, for technical support, Sander Langereis, Ph.D., in collaboration with the Technical University of Eindhoven for cryo-TEM work, Dr. Sennewald Medizintechnik for supply of the hyperthermia device, and Wolfgang Fendler, M.D., from University of Essen for discussion of the PET data. Financial support was obtained by HelmholtzZentrum München, a research grant from the “Dr. Mildred Scheel Stiftung fuer Krebsforschung (Deutsche Krebshilfe e.V.),” by the Federal Ministry of Education and Research of the Federal Republic of Germany under the grant agreements 13XP5014A, 13XP5014B, and 13XP5014C (TSL-LIFU project) and funding from the Deutsche Forschungsgemeinschaft (DFG) under Grant Agreement No. SFB 824.

Conflict of Interest

M.H. and L.H.L. have founder's equity shares in Thermosome GmbH, which develops drug candidates based on phosphatidyl-oligo-glycerols. None of the other authors declare a conflict of interest.

Data Availability Statement

Research data are not shared.

Keywords

drug delivery, hyperthermia, nanomedicines, neoadjuvants, phosphatidyloligoglycerol, soft tissue sarcoma, thermosensitive liposomes

Received: November 24, 2020

Revised: February 18, 2021

Published online: March 31, 2021

- [1] R. A. Gladdy, A. Gupta, C. N. Catton. *Surg. Oncol. Clin. N. Am.* **2016**, *25*, 697.
- [2] A. Gronchi, S. Ferrari, V. Quagliuolo, J. M. Broto, A. L. Pousa, G. Grignani, U. Basso, J.-Y. Blay, O. Tendero, R. D. Beveridge, V. Ferraresi, I. Lugowska, D. F. Merlo, V. Fontana, E. Marchesi, D. M. Donati, E. Palassini, E. Palmerini, R. de Sanctis, C. Morosi, S. Stacchiotti, S. Bagué, J. M. Coindre, A. P. Dei Tos, P. Picci, P. Bruzzi, P. G. Casali. *Lancet Oncol.* **2017**, *18*, 812.
- [3] R. D. Issels, L. H. Lindner, J. Verweij, P. Wust, P. Reichardt, B.-C. Schem, S. Abdel-Rahman, S. Daugaard, C. Salat, C.-M. Wendtner, Z. Vujaskovic, R. Wessalowski, K.-W. Jauch, H. R. Dürr, F. Ploner, A. Baur-Melnyk, U. Mansmann, W. Hiddemann, J.-Y. Blay, P. Hohenberger. *Lancet Oncol.* **2010**, *11*, 561.
- [4] R. D. Issels. *Eur. J. Cancer* **2008**, *44*, 2546.
- [5] R. D. Issels, L. H. Lindner, J. Verweij, R. Wessalowski, P. Reichardt, P. Wust, P. Ghadjar, P. Hohenberger, M. Angele, C. Salat, Z. Vujaskovic, S. Daugaard, O. Mella, U. Mansmann, H. R. Dürr, T. Knösel, S. Abdel-Rahman, M. Schmidt, W. Hiddemann, K.-W. Jauch, C. Belka, A. Gronchi. *JAMA Oncol.* **2018**, *4*, 483.
- [6] M. W. Dewhirst, T. W. Secomb. *Nat. Rev. Cancer* **2017**, *17*, 738.
- [7] B. Seddon, S. J. Strauss, J. Whelan, M. Leahy, P. J. Woll, F. Cowie, C. Rothermundt, Z. Wood, C. Benson, N. Ali, M. Marples, G. J. Veal, D. Jamieson, K. Küver, R. Tirabosco, S. Forsyth, S. Nash, H.-M. Dehbi, S. Beare. *Lancet Oncol.* **2017**, *18*, 1397.
- [8] W. D. Tap, R. L. Jones, B. A. van Tine, B. Chmielowski, A. D. Elias, D. Adkins, M. Agulnik, M. M. Cooney, M. B. Livingston, G. Pennock, M. R. Hameed, G. D. Shah, A. Qin, A. Shahir, D. M. Cronier, Ilaria Robert, Jr, I. Conti, J. Cosaert, G. K. Schwartz. *Lancet* **2016**, *388*, 488.
- [9] I. Judson, J. Verweij, H. Gelderblom, J. T. Hartmann, P. Schoffski, J.-Y. Blay, J. M. Kerst, J. Sufliansky, J. Whelan, P. Hohenberger, A. Krarup-Hansen, T. Alcindor, S. Marreaud, S. Litiere, C. Hermans, C. Fisher, P. C. W. Hogendoorn, A. P. Dei Tos, W. T. A. van der Graaf. *Lancet Oncol.* **2014**, *15*, 415.
- [10] S. Mura, J. Nicolas, P. Couvreur. *Nat. Mater.* **2013**, *12*, 991.
- [11] E. Tahover, Y. P. Patil, A. A. Gabizon. *Anticancer Drugs* **2015**, *26*, 241.
- [12] M. E. O'Brien, N. Wigler, M. Inbar, R. Rosso, E. Grischke, A. Santoro, R. Catane, D. G. Kieback, P. Tomczak, S. P. Ackland, F. Orlandi, L. Mellars, L. Alland, C. Tendler, CAELYX Breast Cancer Study Group. *Ann. Oncol.* **2004**, *15*, 440.
- [13] I. Judson, J. A. Radford, M. Harris, J. Y. Blay, Q. van Hoesel, A. Le Cesne, A. T. van Oosterom, M. J. Clemons, C. Kamy, C. Hermans, J. Whittaker, E. Di Donato Paola, J. Verweij, S. Nielsen. *Eur. J. Cancer* **2001**, *37*, 870.
- [14] S. Wilhelm, A. J. Tavares, Q. Dai, S. Ohta, J. Audet, H. F. Dvorak, W. C. W. Chan. *Nat. Rev. Mater.* **2016**, *1*, 16014.
- [15] C. P. Hollis, H. L. Weiss, M. Leggas, B. M. Evers, R. A. Gemeinhart, T. Li. *J. Control Release* **2013**, *172*, 12.
- [16] S. Sindhvani, A. M. Syed, J. Ngai, B. R. Kingston, L. Maiorino, J. Rothschild, P. MacMillan, Y. Zhang, N. U. Rajesh, T. Hoang, J. L. Y. Wu, S. Wilhelm, A. Zilman, S. Gadde, A. Sulaiman,

- B. Ouyang, Z. Lin, L. Wang, M. Egeblad, W. C. W. Chan. *Nat. Mater.* **2020**, *19*, 566.
- [17] A. L. B. Seynhaeve, B. M. Dicheva, S. Hoving, G. A. Koning, T. L. M. ten Hagen. *J. Control Release* **2013**, *172*, 330.
- [18] M. B. Yatvin, J. N. Weinstein, W. H. Dennis, R. Blumenthal. *Science* **1978**, *202*, 1290.
- [19] B. Kneidl, M. Peller, G. Winter, L. H. Lindner, M. Hossann. *Int. J. Nanomed.* **2014**, *9*, 4387.
- [20] C. D. Landon, J.-Y. Park, D. Needham, M. W. Dewhirst. *Open Nanomed. J.* **2011**, *3*, 38.
- [21] Y. Dou, K. Hynynen, C. Allen. *J. Controlled Release* **2017**, *249*, 63.
- [22] A. A. Manzoor, L. H. Lindner, C. D. Landon, J.-Y. Park, A. J. Simnick, M. R. Dreher, S. Das, G. Hanna, W. Park, A. Chilkoti, G. A. Koning, T. L. M. ten Hagen, D. Needham, M. W. Dewhirst. *Cancer Res.* **2012**, *72*, 5566.
- [23] M. de Smet, N. M. Hijnen, S. Langereis, A. Elevelt, E. Heijman, L. Dubois, P. Lambin, H. Grull. *Invest Radiol.* **2013**, *48*, 395.
- [24] M. C. Sandström, L. M. Ickenstein, L. D. Mayer, K. Edwards. *J. Control Release* **2005**, *107*, 131.
- [25] B. Banno, L. M. Ickenstein, G. N. C. Chiu, M. B. Bally, J. Thewalt, E. Brief, E. K. Wasan. *J. Pharm. Sci.* **2010**, *99*, 2295.
- [26] A. Gabizon, J. Szebeni. *ACS Nano* **2020**, *14*, 7682.
- [27] T. M. Allen, F. J. Martin. *Semin. Oncol.* **2004**, *31*, 5.
- [28] M. Hossann, T. Wang, M. Wiggenhorn, R. Schmidt, A. Zengerle, G. Winter, H. Eibl, M. Peller, M. Reiser, R. D. Issels, L. H. Lindner. *J. Control Release* **2010**, *147*, 436.
- [29] L. H. Lindner, M. E. Eichhorn, H. Eibl, N. Teichert, M. Schmitt-Sody, R. D. Issels, M. Dellian. *Clin. Cancer Res.* **2004**, *10*, 2168.
- [30] X. Li, D. J. Hirsh, D. Cabral-Lilly, A. Zirkel, S. M. Gruner, A. S. Janoff, W. R. Perkins. *Biochim. Biophys. Acta* **1998**, *1415*, 23.
- [31] S. Limmer, J. Hahn, R. Schmidt, K. Wachholz, A. Zengerle, K. Lechner, H. Eibl, R. D. Issels, M. Hossann, L. H. Lindner. *Pharm. Res.* **2014**, *31*, 2276.
- [32] T. M. Allen, A. Chonn. *FEBS Lett.* **1987**, *223*, 42.
- [33] J. J. Mittag, B. Kneidl, T. Preiß, M. Hossann, G. Winter, S. Wuttke, H. Engelke, J. O. Rädler. *Eur. J. Pharm. Biopharm.* **2017**, *119*, 215.
- [34] B. L. Viglianti, M. W. Dewhirst, R. J. Boruta, J.-Y. Park, C. Landon, A. N. Fontanella, J. Guo, A. Manzoor, C. L. Hofmann, G. M. Palmer. *Int. J. Hyperthermia* **2014**, *30*, 385.
- [35] M. de Smet, S. Langereis, S. van den Bosch, K. Bitter, N. M. Hijnen, E. Heijman, H. Grull. *J. Control Release* **2013**, *167*, 82.
- [36] L. Li, T. L. M. ten Hagen, M. Bolkestein, A. Gasselhuber, J. Yatvin, G. C. van Rhoo, A. M. M. Eggermont, D. Haemmerich, G. A. Koning. *J. Control Release* **2013**, *167*, 130.
- [37] L. Willerding, S. Limmer, M. Hossann, A. Zengerle, K. Wachholz, T. L. M. ten Hagen, G. A. Koning, R. Sroka, L. H. Lindner, M. Peller. *J. Controlled Release* **2016**, *222*, 47.
- [38] I. W. Mak, N. Evaniew, M. Ghert. *Am. J. Transl. Res.* **2014**, *6*, 114.
- [39] S. S. Couto, S. M. Griffey, P. C. Duarte, B. R. Madewell. *Vet. Pathol.* **2002**, *39*, 33.
- [40] A. Dhaliwal, G. Zheng. *Theranostics* **2019**, *9*, 8091.
- [41] V. J. Poirier, D. H. Thamm, I. D. Kurzman, K. A. Jeglum, R. Chun, J. E. Obradovich, M. O'Brien, R. M. Fred, B. S. Phillips, D. M. Vail. *J. Vet. Intern. Med.* **2002**, *16*, 726.
- [42] W. P. Fendler, M. Lehmann, A. Todica, K. Herrmann, T. Knösel, M. K. Angele, H. R. Dürr, J. Rauch, P. Bartenstein, C. C. Cyran, M. Hacker, L. H. Lindner. *J. Nucl. Med.* **2015**, *56*, 530.
- [43] K. Zimmermann, M. Hossann, J. Hirschberger, K. Troedson, M. Peller, M. Schneider, A. Bruhschwein, A. Meyer-Lindenberg, G. Wess, M. Wergin, R. Dorfelt, T. Knösel, M. Schwaiger, C. Baumgartner, J. Brandl, S. Schwamberger, L. H. Lindner. *Int. J. Hyperthermia* **2017**, *33*, 178.
- [44] A. I. Minchinton, I. F. Tannock. *Nat. Rev. Cancer* **2006**, *6*, 583.